Microstructure Prediction of 80MnSi8-6 Steel After Hot Deformation Based on Dynamic Recrystallization Kinetics and FEM Simulation

KRYSTIAN ZYGUŁA [ORCID],[1,5] KAMIL CICHOCKI,[1] KAROLINA KOWALCZYK,[2] MICHAŁ PUŁAWSKI,[3] GRZEGORZ KORPAŁA,[3] MAREK WOJTASZEK,[1] MAGDALENA JABŁOŃSKA,[4] and ULRICH PRAHL[3]

1.—Faculty of Metals Engineering and Industrial Computer Science, AGH University of Krakow, Al. Mickiewicza 30, 30-059 Kraków, Poland. 2.—Institute of Materials Engineering, University of Silesia, 75 Pułku Piechoty 1a, 41-500 Chorzów, Poland. 3.—Institut für Metallformung, TU Bergakademie Freiberg, 4 Bernhard-von-Cotta-Straße, 09599 Freiberg, Germany. 4.—Faculty of Materials Engineering, Silesian University of Technology, Krasińskiego 8, 40-019 Katowice, Poland. 5.—e-mail: kzygula@agh.edu.pl

The microstructure evolution during hot deformation of 80MnSi8-6 nanobainitic steel was investigated through hot compression tests at deformation temperatures of 900–1250°C and strain rates of 0.1–20 s^{-1}. The flow curves revealed strain-hardening behavior at the beginning of deformation followed by softening effects caused by microstructure evolution. A Johnson–Mehl–Avrami–Kolmogorov (JMAK) model for grain growth and dynamic recrystallization was developed, and the kinetics were determined. Critical and peak strains were identified, and coefficients for the microstructure evolution models were determined using linear regression. The analysis of S-curves revealed that decreasing the temperature delays the onset of recrystallization and that the strain rate significantly effects the recrystallization rate at lower temperatures. Constitutive modeling and determination of the Zener–Hollomon parameter allowed the determination of the influence of hot processing conditions on material behavior during deformation. Microstructure analysis showed that, at higher deformation temperatures, grain growth occurs simultaneously with grain refinement. Coefficients for the JMAK model were implemented in QForm software. Simulation results were compared with experimental measurements exhibited good arrangement, which confirms the accuracy of the JMAK model in predicting the microstructure evolution. This study demonstrated how microstructure evolution modeling and FEM simulations combined can be used to predict the grain size of 80MnSi8-6 steel after hot deformation.

INTRODUCTION

The description of material behavior during hot deformation is highly significant yet quite complex due to the accompanying phenomena. It is possible to distinguish the following processes: grain growth, work hardening (WH), dynamic recovery (DRV), and dynamic recrystallization (DRX).[1,2] All these phenomena significantly influence the flow stress and microstructure evolution. Analyzing the flow stress curves obtained from hot compression tests helps in understanding the material's behavior and enables the identification of the occurrence of phenomena related to microstructure evolution. Describing the correlations between hot deformation parameters, such as temperature, strain, and

strain rate, and the microstructural changes mostly associated with DRX, is crucial in the design and optimization of plastic deformation processes such as hot forging.

In recent years, the subject of DRX kinetics has been frequently investigated by researchers. Such studies are important because metal alloys and steels are sensitive not only to changes in deformation parameters but also to modifications in chemical composition.[3,4] That is why there is a high demand for analysis of the hot deformation behavior of metallic materials. For instance, Liu et al.[5] presented a classical approach to calculating the kinetics of recrystallization in ferritic–martensitic steel, enriched with a model that allows for determine the average grain size of austenite and processing maps. Guo et al.[6] undertook the determination of recrystallization kinetics for steels for which no clear peak stress is observed on the flow curves at high strain rates. This complicates the determination of the onset of DRX. Kumar et al.[7] investigated the effect of nitrogen on the recrystallization kinetics of Fe-Cr-Ni-Mo steel. Calculations based on flow stress curves and accompanying microstructure observations after deformation under various conditions showed that an increase in nitrogen content reduces the critical strain for recrystallization and changes the behavior of DRX. This leads to the generation of more dislocations within the grains, resulting in an increased number of nucleation sites for new DRX grains and, consequently, a finer microstructure. A great effort has also been made to determine recrystallization kinetics for materials other than steel. DRX analysis based on flow stress curves has also been conducted for titanium,[8] magnesium,[9] or aluminum alloys,[10] often enriched with constitutive equations.[11] Determining DRX kinetics can contribute to the development of models like the Johnson–Mehl–Avrami–Kolmogorov (JMAK) model.[12] A well-developed model implemented into finite element method (FEM) software is valuable for predicting grain size changes during plastic deformation processes, eliminating the need for extensive laboratory or industrial tests.[13] This results in financial and time savings for companies that manufacture steel or other metal products. However, the process is relatively complex due to the challenging and time-consuming optimization of correlations between experimental results, computational analysis, and simulations, making it less frequently undertaken.

Nanobainitic steel is a relatively new material that has been under development since the beginning of the twenty-first century. It has found application in the production of large-sized components that undergo prolonged cooling times and exhibits exceptionally high strength while maintaining plasticity. The excellent properties of nanobainitic steels are the result of their unique chemical and phase composition. The high content of carbon and silicon lowers the temperature of the bainitic transformation, which strengthens the austenite and makes it possible to obtain very thin plates of bainitic ferrite. During the isothermal holding process, nanostructured plates of bainitic ferrite of about 50 nm in size are formed, arranged alternately with the retained austenite.[14] As a result, nanobainitic steels have tensile strengths as high as 2 GPa with an elongation of about 20%.[15] Unfortunately, obtaining bainite or nanobainite through the austempering process is highly time-consuming, taking up to 4 days, making its industrial implementation uneconomical.[16] In order to accelerate bainitic transformation, some concepts have been proposed to modify the chemical composition of the material. One approach involves replacing the manganese with nickel, which, although more expensive, has shown potential to enhance the transformation kinetics.[17] Other studies have suggested the addition of cobalt and aluminum, along with a reduction in carbon content.[18,19] These solutions shorten the transformation time to 1 day, but they increase the material cost, thus the problem of cost-effectiveness remains unsolved. Bhadeshia[20] conducted research on the influence of the austenite state (deformed, recrystallized, or fine-grained) on the bainitic transformation rate. The obtained results concerning the effects of adding cobalt and aluminum and achieving very fine-grained austenite were promising but still insufficient. Moreover, deformed but non-recrystallized austenite hindered the bainitic transformation. This effect is known as the mechanical stabilization of austenite. A very promising approach to accelerate nanobainite formation was presented by Garcia-Mateo et al.[21] who proposed inducing external stresses during the bainitic transformation. The transformation time can be reduced to just a few minutes by applying tensile or compressive stresses, but their application during bainite transformation in large, forged shapes can be problematic. However, a simple way to introduce these stresses is through torsional shear stress. This stress state allows for the separation of volumetric changes and plasticity induced by transformation, providing an opportunity to understand the essence of the Gibbs energy balance associated with mechanical stabilization of austenite (high dislocation density),[22] stress-induced transformation,[23] and chemical driving force.[24]

The properties of high-carbon forged steels, such as nanobainitic steels, are limited due to their susceptibility to cracking. Therefore, accurately defined and applied thermomechanical processing parameters are crucial for effective forging cycle design. This study has focused on investigating the microstructure evolution of 80MnSi8-6 nanobainitic steel during hot deformation. Hot compression tests were conducted at different temperatures ranging from 900°C to 1250°C and various strain rates between 0.1 and 20 s^{-1}. This range of parameters

Microstructure Prediction of 80MnSi8-6 Steel After Hot Deformation Based on Dynamic
Recrystallization Kinetics and FEM Simulation

5195

was chosen to ensure deformation in the austenite range and to be able to investigate the influence of deformation conditions on the size of prior austenite grains (PAGs). The proposed temperatures can be applied to the open die hot forging process under industrial conditions. A grain growth and DRXmodel based on the JMAK model was developed to describe the microstructure changes. The kinetics of DRX were determined by analyzing the flow curves and identifying critical and peak strain points. The coefficients for the microstructure evolution models were obtained through linear regression. Microstructure analysis involved revealing the PAGs. The JMAK model was then implemented in QForm software, allowing for simulations that were subsequently compared to the experimental results. This approach facilitated the prediction of the microstructure evolution of 80MnSi8-6 steel after hot deformation. By understanding and accurately predicting the microstructural changes during hot deformation, it is possible to tailor the final grain size, and, consequently, influence the properties of the final product.

EXPERIMENTAL

80MnSi8-6 steel with the chemical composition presented in Table I was used for the study. The material was obtained through casting processes followed by preliminary open die hot forging. To determine the PAG size for the grain growth model, the samples were heated to temperatures of 900°C, 1150°C, and 1250°C, held for 0 s, 30 s, 60 s, 120 s, and 240 s, and then quenched in water. Subsequently, the samples were sectioned, polished, and etched to reveal the PAG boundaries. Microstructure observations were carried out using a setup equipped with an automated image analysis system consisting of a NIKON X light microscope and dedicated to metallographic stereology Metilo® software for quantitative image analysis.[25] Image acquisition on the light microscope was performed at magnifications of × 100, × 200, and × 500 using bright-field techniques. To eliminate the shadow effect, present in the recorded images, a procedure called the correction function was applied. This procedure allowed for the proper identification of grain boundaries and enabled the application of automatic image binarization, with occasional manual corrections for accurate indication of the revealed microstructural boundaries. This approach facilitated the determination of the average

diameter of the austenite grains in the analyzed images. Measurements were carried out based on a series of three images for each sample.

Cylindrical samples with a diameter of 12 mm and a height of 18 mm were cut from the investigated steel for hot compression tests. The tests were conducted using a thermo-mechanical deformation simulator, WUMSI, at temperatures of 900°C, 1000°C, 1100°C, and 1250°C, with strain rates of 0.1 s^{-1}, 1 s^{-1}, 10 s^{-1}, and 20 s^{-1}. To minimize the friction effect during hot deformation, the top and bottom surfaces were covered using graphite lubricant. The samples were heated up in heat-resistant steel compression containers in a furnace to 1250°C and held for 10 min to ensure microstructure homogenization. Based on data from the thermocouples that controlled the temperature during heating, the heating rate was determined to be 5°C/s. After reaching the desired temperature, the samples were cooled to the desired test temperature, deformed to a strain of 1.2, then taken out of the compression containers and quenched in water. The hot compression test schedule is shown in Fig. 1. After compression, the samples were cut along the axis parallel to the compression direction. The metallographic procedure, microstructure observations, and grain size analysis were conducted similarly to the samples for the grain growth. Grain size measurements were performed based on a series of three images for each sample. The central part of the samples was the area where microstructure observations of the investigated steel were carried out.

The FEM simulations were conducted using commercially available QForm 10.2.1 software. During simulation, the elastic range of deformation was not considered and deformed material was treated as an incompressible isotropic continuum. The software conducted computations using a structured viscous model incorporating reinforcements. In this model, the flow stress was determined by considering the extent of strain, strain rate, and temperature. The calculations also incorporated heat generated during the deformation process. Levanov's law[26] was employed to characterize friction in the system. To accurately replicate the hot compression process and material behavior, machine characteristics and material properties such as flow stress curves, chemical composition, as well as density, thermal conductivity, and specific heat as a function of temperature, were implemented in the software's database. To simulate the grain size change during

Table I. Chemical composition of 80MnSi8-6 steel (wt.%)

C	Si	Mn	P	S	Cr	Mo	V	Fe
0.79	1.55	1.9	0.003	0.003	1.3	0.25	0.11	Balance

heating and deformation, coefficients of the grain growth model as well as static, dynamic, and meta-DRX models based on the JMAK model were implemented in the software. These models allowed for the accurate prediction of grain evolution during the hot compression process.

RESULTS AND DISCUSSION

Grain Growth Kinetics

Grain growth phenomena occur while heating and annealing the material before deformation. It can also take place during or after deformation if the material is not subjected to external forces causing deformation and if temperature is high
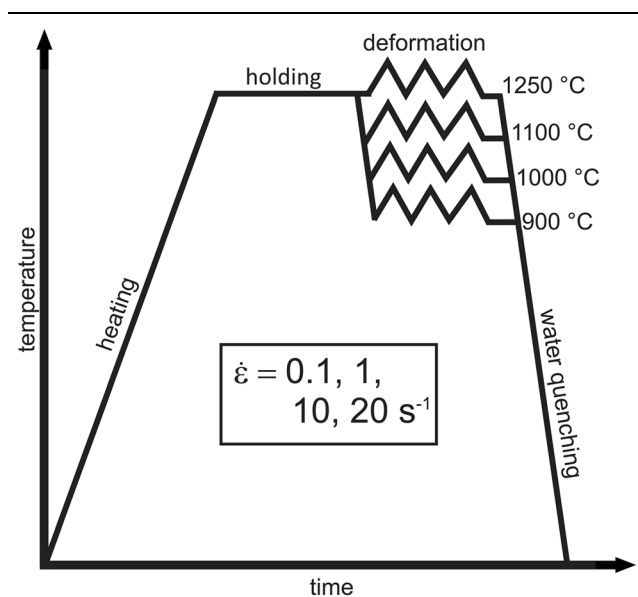

Fig. 1. Experimental procedure for hot compression tests.

enough. The driving force behind this process is the reduction of grain boundary energy by minimizing the grain boundary area or defects.[27,28] Figure 2 shows selected microstructures of the 80MnSi8-6 steel samples after annealing at temperatures of 900°C, 1150°C, and 1250°C with grain boundaries highlighted by Metilo® software as well as corresponding grain size distributions. As expected, with an increase in temperature and annealing time, the grain size increases. Temperature and annealing time are crucial parameters that significantly influence the process of austenite grain growth and its size. Proper selection of these parameters allows achieving the desired material properties and impacts the subsequent processing. Fernandez et al.[29] correctly noted that, as PAGs increase, there is a reduction in the number of available nucleation sites at the grain boundary. This will have the effect of lowering the DRX rate and increasing peak strain. By understanding the kinetics of grain growth, it is possible to tailor the annealing parameters to precisely control the grain size directly before hot deformation, which affects the final grain size. For instance, annealing at the lowest temperature with a holding time of 30 s (Fig. 2a) gives the same effect as annealing at 1150°C (Fig. 2c) without any holding time. Grain size measurement results for temperatures of 900°C, 1150°C, and 1250°C, and holding times of 0 s, 30 s, 60 s, 120 s, and 240 s (Fig. 3, symbols) were incorporated into the grain growth model calculations.

The grain growth kinetics is generally described by Eq. 1, that can be written as:[30]

$$d_{gg}^{m_{gg}} - d_0^{m_{gg}} = ct \qquad (1)$$

where d_{gg} is the mean grain size at the annealing temperature and time, d_0 is the initial mean grain
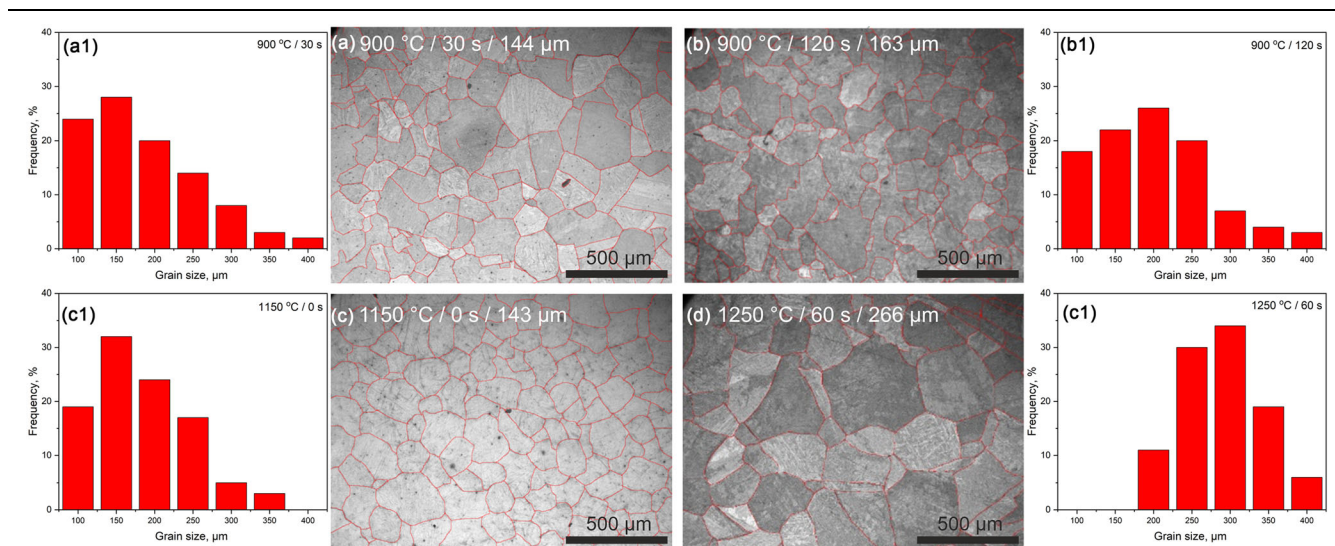

Fig. 2. Microstructures of 80MnSi8-6 steel after annealing at (a) 900°C/30 s, (b) 900°C/120 s, (c) 1150°C/0 s and (d) 1250°C/240 s with applied PAG analysis results by Metilo® software and corresponding grain size distributions for each annealing conditions (a1–d1).
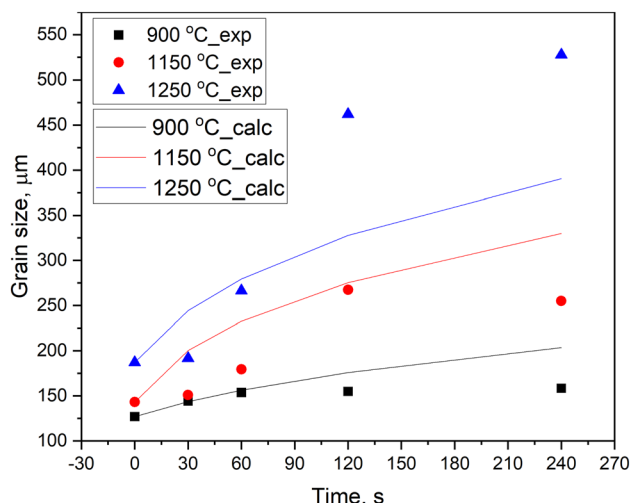
Microstructure Prediction of 80MnSi8-6 Steel After Hot Deformation Based on Dynamic
Recrystallization Kinetics and FEM Simulation

5197

Fig. 3. Comparison between experimental (symbols) and calculated
(lines) mean grain sizes after annealing.

size at $t = 0$, m_{gg} is the grain growth exponent, and c
is a grain growth rate constant, and can follow the
Arrhenius-type equation:

$$c = A_{gg}\exp\left(-\frac{Q_{gg}}{RT}\right) \qquad (2)$$

where A_{gg} is a material constant, Q_{gg} is the activa-
tion energy, R is the universal gas constant, and T is
the annealing temperature. As evident from Fig. 3,
at a temperature of 900°C and at the initial time,
the austenite grain size increases to a certain value,
and then the growth rate stabilizes at a low level
with increasing time. For temperatures of 1150°C
and 1250°C, the grain size gradually grows with the
increase in time. A particularly pronounced grain
size increase is observed during annealing at
1250°C between 60 and 120 s, reaching over
125 μm. Considering the above, a combined grain
size model after annealing can be deduced, taking
into account Eqs. 1 and 2, expressed as:

$$d_{gg} = \left[d_0^{m_{gg}} + A_{gg} \cdot t \cdot \exp\left(-\frac{Q_{gg}}{RT}\right)\right]^{\frac{1}{m_{gg}}} \qquad (3)$$

The m_{gg} constant can be calculated by linear
regression using experimental data from quantita-
tive microstructure analysis of PAGs. In Fig. 4a the
relationship between $\ln(d_{gg})$ versus $\ln(t)$ is pre-
sented. The mean value of slope of each curve allows
the calculation of the m_{gg} exponent, which is 3.55.
Similarly, taking the $\ln(d_{gg})$ with respect to
$1000/T$, the Q_{gg} can be calculated by multiplying
the absolute value of the mean slope and R (Fig. 4b).
The mean value of grain growth activation energy is
equal to 103.7 kJ/mol. By substituting the values of
m_{gg} and Q_{gg} in Eq. 3, the value of A_{gg} can be
calculated.[31,32] Equation 3 was implemented in the
QForm software for calculation of the grain size

after grain growth phenomenon. The coefficients
used in the QForm software are shown in Table S8
(refer to online supplementary material).

Figure 3 presents a comparison between the
experimentally determined average grain size and
the size calculated based on the developed model.
Both the experimental data and the model indicate
that the grain growth generally follows exponential
behavior. At the temperatures of 1250°C after 60 s,
the experimental data slightly deviate from this
trend, which could signify sudden changes in the
microstructure that the model developed for the full
range of data cannot incorporate. Such a phe-
nomenon has been observed before, and many
researchers have proposed explanations. Cota
et al.[33] observed rapid grain growth after dissolu-
tion of niobium carbonitrides above 1100°C in
micro-alloyed steel. Meanwhile, a similar effect
was confirmed by Zhang and Kannengiesser[34] for
HSLA steel, where, above 1100°C, there was disso-
lution of niobium carbonitrides and AlN caused
accelerated austenite grain growth. Ivaniski et al.[35]
studied grain size evolution in bainitic steel during
hot forging, and associated the rapid grain growth
at 1200°C with the dissolution of precipitates
formed by micro-alloying elements such as Ti, N,
and Al. However, carbide dissolution in the inves-
tigated steel is unlikely, since nanobainitic steels
are considered carbide-free. In addition, the high Si
content of the 80MnSi8-6 steel should effectively
block carbide precipitation and coalescence. Kró-
licka et al.[36] directly excluded the effect of carbide-
forming additives on grain growth during anneal-
ing, attributing the rapid grain growth above
1100°C to the abnormal grain growth phenomenon.
As noted, in nanobainitic steels, the absence of
carbide-forming additives and the inhibition of
carbide precipitation in bainite by high Si content
results in the absence of high-melting precipitates
that could inhibit grain boundary growth. In this
case, the disappearance of obstacles hindering the
movement of grain boundaries leads to a noticeable
increase in grain size, which is reflected in the
relatively low average value of Q_{gg}. Generally, the
activation energy for grain growth in low-alloy,
high-carbon steels is relatively low. Lee et al.[37]
demonstrated that, with the increase in tempera-
ture above 1200°C, the activation energy dramati-
cally decreased. This was related to the dissolution
of carbon in the austenite, which as an interstitial
element is responsible for controlling the growth of
austenite grains. Carbon dissolved in austenite
reduces the binding energy between iron atoms,
thereby facilitating grain growth.[38] Carbon also
plays an important role in grain boundary segrega-
tion, which can be an inhibitor of the DRX process.[39]
Additionally segregation of carbon to austenite
grain boundaries strongly influences the subse-
quent formation of bainite.[40] Therefore, the phe-
nomenon of grain growth involves several
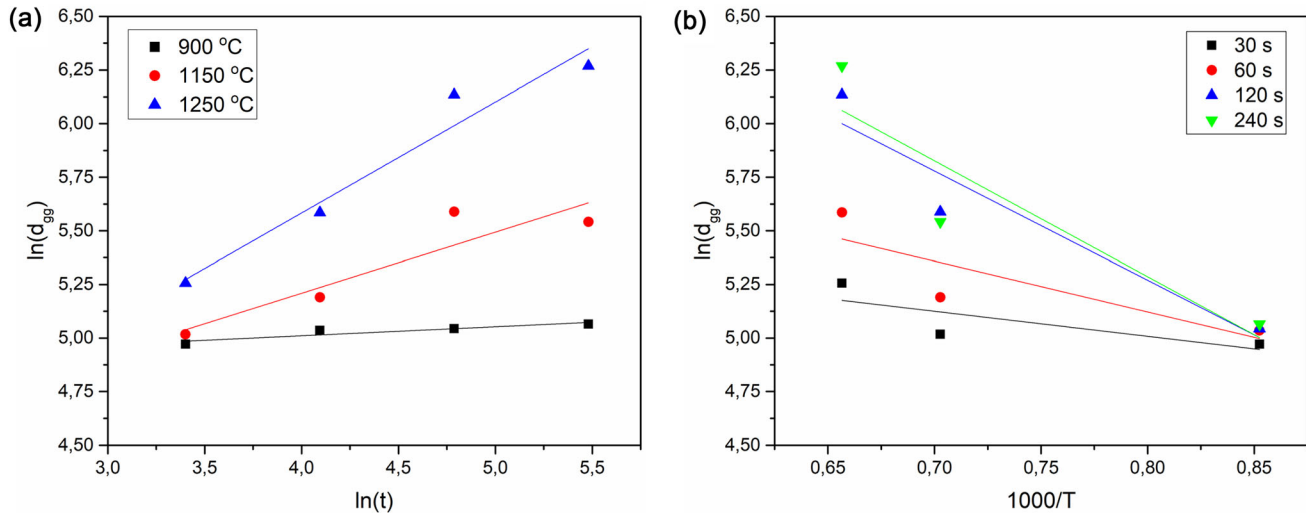mechanisms operating simultaneously, which are

Fig. 4. The relationship between (a) $\ln(d_{gg}) - \ln(t)$ and (b) $\ln(d_{gg}) - 1000/T$.

also linked to complex diffusion processes. As evidenced by the study findings, the determining factor affecting the size of PAGs is primarily temperature, followed by the duration of exposure.

Flow Curves

The true stress–strain curves of 80MnSi8-6 steel deformed at different temperatures and strain rates are presented in Fig. 5. To accurately determine the true stress during the hot compression test, corrections considering the influence of frictional force and adiabatic heating must be applied. These necessary corrections were calculated during the development of the flow stress curves using the Hensel–Spittel method and the Siebel equation.[41,42] Material data, such as the friction coefficient during hot deformation, the density, and the thermal conductivity of the investigated material, were used during the curve correction process to accurately determine the true flow stress.

The flow curves demonstrate that the 80MnSi8-6 steel exhibits typical strain rate and temperature sensitivity. The flow stress increases rapidly during the initial stages of deformation, which is associated with the generation and accumulation of dislocations at the grain boundaries, which is known as WH. This state remains until reaching the peak strain (ε_p), where the highest stress, known as peak stress (σ_p), is observed. The peak stress is more pronounced at lower deformation temperatures or higher deformation rates. It was also observed that, for the investigated steel, both peak strain and related peak stress occur relatively late. Subsequently, with further increase of strain, there is a decrease in stress as high-temperature microstructure evolution mechanisms such as DRV and DRX (known as deformation softening effects) occur simultaneously, counteracting the effects of the WH. The DRV is activated even before the stress

curve reaches peak stress, resulting in a slowing down of the stress increase before ε_p is reached. DRX leads to the annihilation of dislocations and the nucleation of new grains. The last stage is the steady-state flow, during which the material flows at a constant stress, and the effects related to WH and deformation softening reach an equilibrium state. At this stage, the material exhibits stable flow behavior, characterized by a constant flow stress, as the effects of WH and deformation softening balance each other out. For temperatures of 1100°C and 1250°C at low strain rates (0.1 s^{-1} and 1 s^{-1}), the flow curves reach equilibrium relatively early, that is, already at a strain equal to 0.4. For temperatures of 900°C and 1000°C, such an effect is evident only for strain rates of 0.1 s^{-1}. Regardless of the deformation temperature, for high strain rates (10 s^{-1} and 20 s^{-1}), a continuous decrease in flow stress with increasing strain is evident. Only for the two highest temperatures is a stabilization above a strain of 1.0 apparent.

DRX Kinetics

The development of DRX kinetics requires accurate determination of characteristic points on the flow stress curve, such as critical stress σ_c, peak stress σ_p, saturation stress σ_s, and steady-state stress σ_{ss}. These characteristic stress values can be determined from the flow curve by calculating the derivative using:[43]

$$\theta = \frac{\partial \sigma}{\partial \varepsilon} \qquad (4)$$

where θ represents the WH rate and is the derivative of the flow stress curve. Figure 6a shows exemplary θ curves as a function of σ at the temperature of 1000°C and different strain rates. To start with, the value of θ decreases rapidly due to the occurrence of the DRV at the beginning of

Microstructure Prediction of 80MnSi8-6 Steel After Hot Deformation Based on Dynamic Recrystallization Kinetics and FEM Simulation
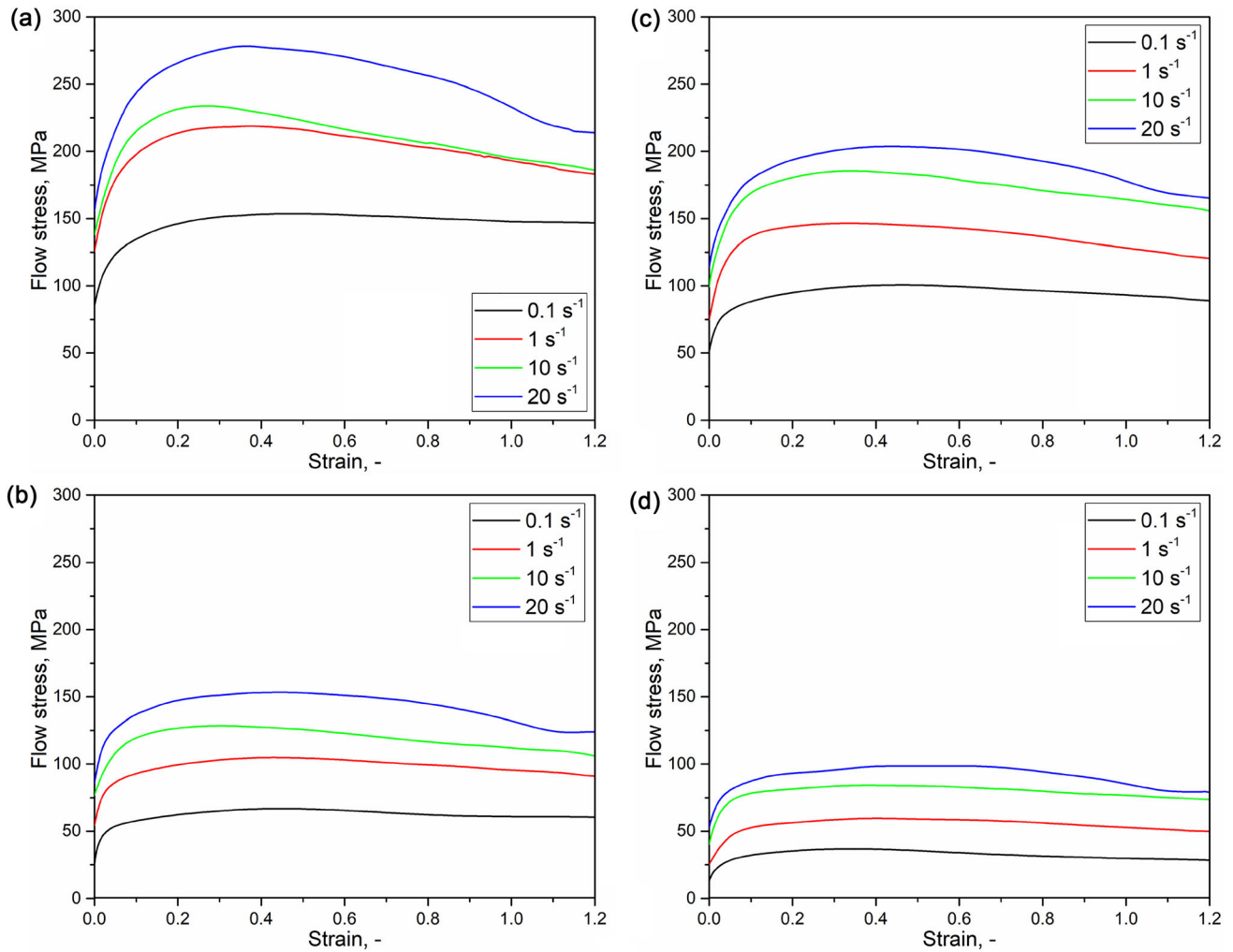
5199

Fig. 5. Stress–strain curves of 80MnSi8-6 steel samples deformed at temperatures of (a) 900°C, (b) 1000°C, (c) 1100°C, and (d) 1250°C.
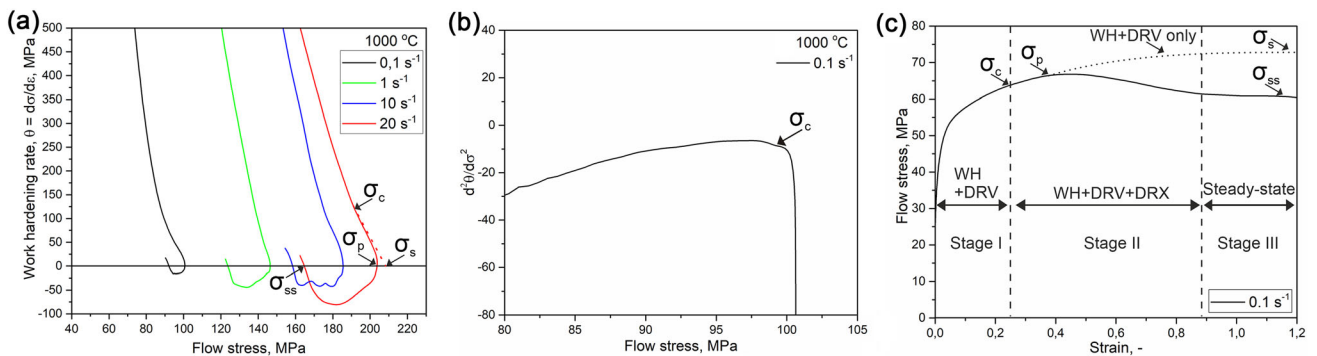

Fig. 6. The relationship of (a) $\theta-\sigma$ for a temperature of 1000°C with schematically indicated characteristic stress values, (b) $d^2\theta/d\sigma^2-\sigma$, and (c) scheme for different deformation stages illustrated on the stress–strain curve of the 80MnSi8-6 steel sample deformed at a temperature of 1100°C and strain rate 0.1 s^{-1}.

plastic deformation. At the point of the first distinct inflection of the curve, the critical point occurs, where the softening rate increases, indicating the initiation of the DRX. This critical point is indicated as σ_c. To accurately determine the characteristic σ_c value, the double differentiation of the work hardening rate θ method was used with respect to stress, as described by Eq. 5,[44] while an exemplary curve is shown in Fig. 6b:

$$0 = \frac{\partial^2 \theta}{\partial^2 \sigma} \qquad (5)$$

If DRX does not occur, and the only softening mechanism is DRV, the θ curve behaves as it is schematically shown by the dashed line in Fig. 6a for a strain rate of 20 s^{-1}. Extrapolating the dashed line to a value of 0 allows for the determination of σ_s. Then, when $\theta = 0$, the flow stress curve reaches the peak stress (σ_p). Afterward, the WH rate reaches a minimum and starts to rise again until it reaches 0, which is the point where a balance between WH, DRV, and DRX is achieved. At this point, steady-state flow (σ_{ss}) is reached.

Based on the behavior of the studied material during the hot deformation, a universal deformation scheme and the accompanying phenomena can be developed, as shown in Fig. 6c. Stage I begins at the start of deformation and lasts until the critical strain, ε_c, is reached. The increase in flow stress is associated with WH, and, towards the end of this stage, the WH rate decreases, and sub-grains begin to form, indicating the occurrence of DRV. Stage II is associated with the onset of DRX. The flow stress significantly decreases, and nucleation and growth of new grains occur, with substantial amounts of dislocations being absorbed. In Stage III, the state of equilibrium is achieved, and the material flows at a constant flow stress.

Knowing the deformation softening scheme, it is possible to determine the volume faction of the DRX based on Eq. 6 and calculate the strain value for 50% recrystallization $\varepsilon_{0.5}$:

$$X_{DRX} = \frac{\Delta\sigma}{\sigma_s - \sigma_{ss}} = \frac{\sigma_p - \sigma}{\sigma_s - \sigma_{ss}} \qquad (6)$$

The kinetics of DRX are commonly described using the so-called S-curves, which represent the volume of recrystallized grains as a function of time, or, in the case of a constant strain rate, as a function of strain. The fraction of recrystallized grain volume can be expressed using a modified Avrami equation:[45]

$$X_{DRX} = 1 - \exp\left(-\beta\left(\frac{\varepsilon - \varepsilon_c}{\varepsilon_{0.5} - \varepsilon_c}\right)^k\right) \qquad (7)$$

where β equals $\ln(1 - X_{50\%})$, which is 0.693. Taking the logarithm of both sides, Eq. 8 can be obtained, and, using values calculated by Eq. 7, the k value can be obtained as shown in Fig. 7. The mean slope value of $\ln(\varepsilon - \varepsilon_c) - \ln\left(-\ln(1/(1 - X_{DRX}))\right)$ for different deformation conditions was 3.5.

$$\ln(-\ln(1 - X_{DRX})) = \ln 0.693 + k\ln\left(\frac{\varepsilon - \varepsilon_c}{\varepsilon_{0.5} - \varepsilon_c}\right) \quad (8)$$

Substituting the known value of ε_c and the determined material constants into Eq. 7 allows for the development of DRX curves, as shown in Fig. 8. Regardless of the temperature and strain rate, all the DRX kinetics curves exhibit a typical S-shaped profile. With increasing strain, the volume fraction of DRX grains increases and, depending on

the deformation parameters, reaches a value of 1 or close to it, which corresponds to steady-state flow. This state represents an equilibrium between accumulated dislocations and their annihilation associated with the nucleation of new grains. Taking the deformation parameters into consideration, the behavior of DRX during hot deformation can be considered in two different manners by taking into account the influence of temperature or of strain rate. In Fig. 8a, the influence of temperature on the degree of recrystallization of the investigated steel during deformation at a strain rate of 0.1 s^{-1} can be seen. A typical relationship is observed where the critical strain for recrystallization decreases with increasing temperature, resulting in a faster recrystallization rate. It can also be observed that the S-curves are clearly divided into two groups. The recrystallization at temperatures of 900°C and 1000°C occurs at similar rates and noticeably later than for temperatures of 1100°C and 1250°C. Also, for these higher temperatures, a similar rate of recrystallization proceeding at a strain rate of 0.1 s^{-1} is evident. Thus, it can be assumed that 1100°C is the critical temperature for microstructural changes during the processing of the investigated steel. Similar conclusions were drawn from the analysis of grain growth kinetics, where increasing the annealing temperature to 1100°C increased the grain growth rate. Figure 8b shows S-curves at the strain rate of 20 s^{-1} for different temperatures, from which it can be seen that an increase in the strain rate reduced the effect of temperature on recrystallization. Regardless of the temperature at this strain rate, the material recrystallizes at a similar rate. What is important is that it was also observed that the recrystallization for a strain rate of 20 s^{-1} is not complete while for a strain value of 1.2 it is about 90 %, and, for a strain rate of 0.1 s^{-1} for each temperature, basically complete recrystallization was observed.

In Fig. 8c and d, the influence of strain rate on DRX behavior at a constant temperature has been analyzed. In this case, depending on the deformation temperature, two different material responses to the increase in strain rate were observed. At low temperatures, the DRX rate is faster at high strain rates, and it decreases with decreasing strain rate. An opposite trend is observed at the highest temperature of 1250°C, where the DRX rate decreases with increasing strain rate. The analysis of Fig. 8 indicates that combinations of the strain rate and temperature parameters have a complex influence on the DRX process. At lower temperatures, the material is more sensitive to strain rate, and the energy delivered for the nucleation of new grains due to high strain rate has a greater significance than temperature. On the other hand, high temperature and prolonged exposure to it cause DRX to occur earlier even at low strain rates, as typically observed in other steels.[46] Similar behavior was observed by Mandal et al.[47] who studied the DRX
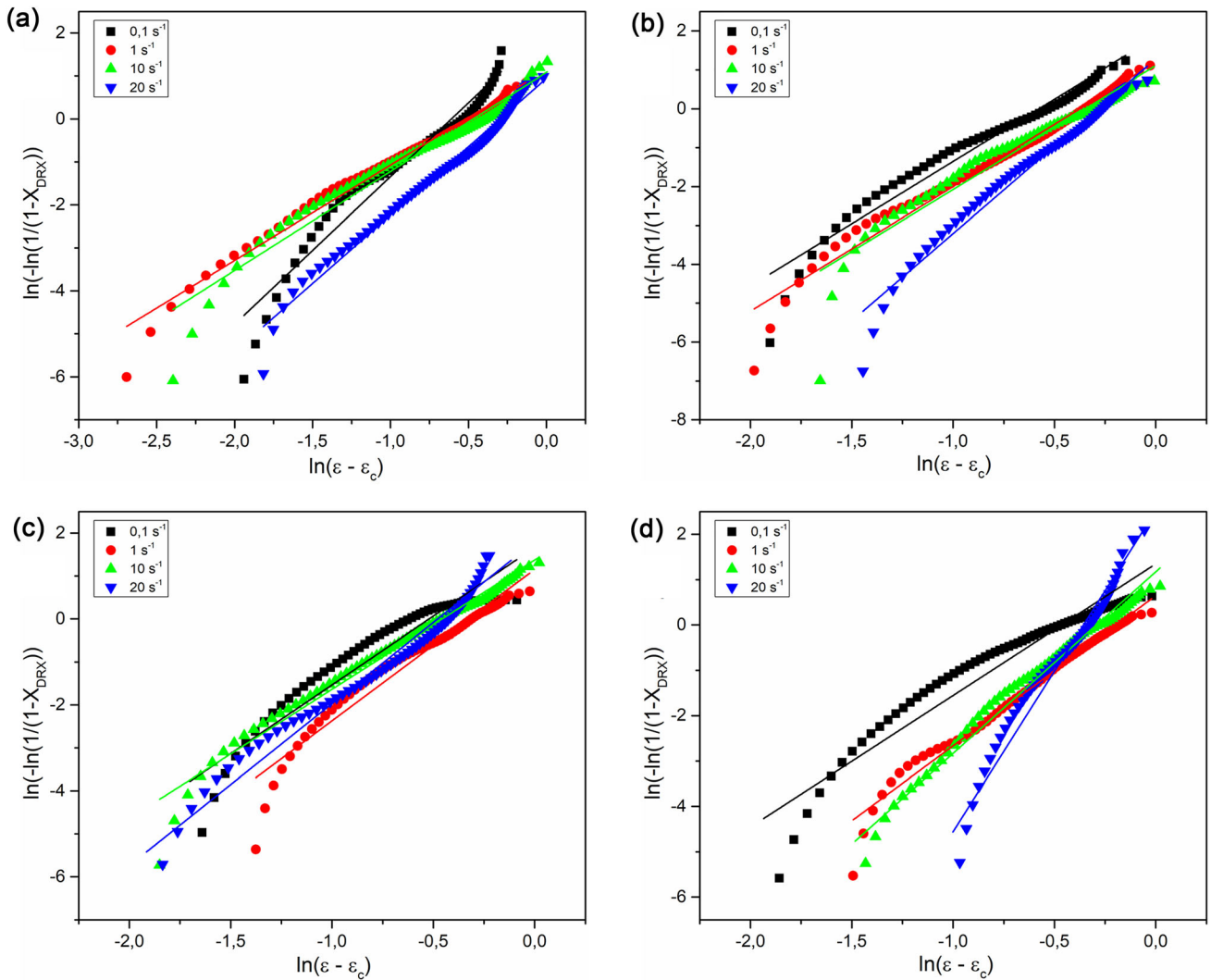
Fig. 7. The relationship between $\ln(\varepsilon - \varepsilon_c) - \ln(-\ln(1/(1 - X_{DRX})))$ for temperatures of (a) 900°C, (b) 1000°C, (c) 1100°C, and (d) 1250°C.

behavior of 316L steel with elevated nitrogen content during hot deformation, particularly focusing on strain rate. They demonstrated that strain rate has a complex influence on DRX kinetics during deformation and categorized its influence into two fundamental domains: low strain rate values and high strain rate values. Based on EBSD analysis, they demonstrated that, for high strain rates, the dislocation density is higher in samples deformed at higher strain rates due to the greater energy stored in those samples. Similar conclusions were reached by Jiang et al.[48] who studied nickel-based alloy 617B. In this alloy, the DRX rate also accelerates at both low and high strain rates. It was observed that higher strain rates generate more energy and dislocation density, which promote DRX nucleation.

Additionally, the earlier investigation of the flow curves revealed that both ε_c and ε_p occur relatively late, regardless of the applied deformation parameters, which also corresponds with the DRX rate analysis. The reason for this may lie in the large grain size resulting from the annealing process before deformation. The nucleation sites for new DRX grains are grain boundaries where energy accumulates due to the piling up of dislocations during deformation. If the austenite grain is large, it is evident that there are fewer grain boundaries available for nucleation of new DRX grains, resulting in a slower recrystallization rate.

There is a widely accepted concept that thermally activated stored energy, developed during the hot deformation process, governs softening mechanisms such as DRX. The key material parameter is the activation energy of DRX, which defines the critical conditions for initiating this process. Several empirical equations have been presented in the literature to determine the activation energy in the hot deformation of metals and to analyze their behavior. In particular, the commonly used Arrhenius equation introduces the Zener–Hollomon parameter (Z) as a measure of the influence of temperature and strain rate on material behavior during deformation
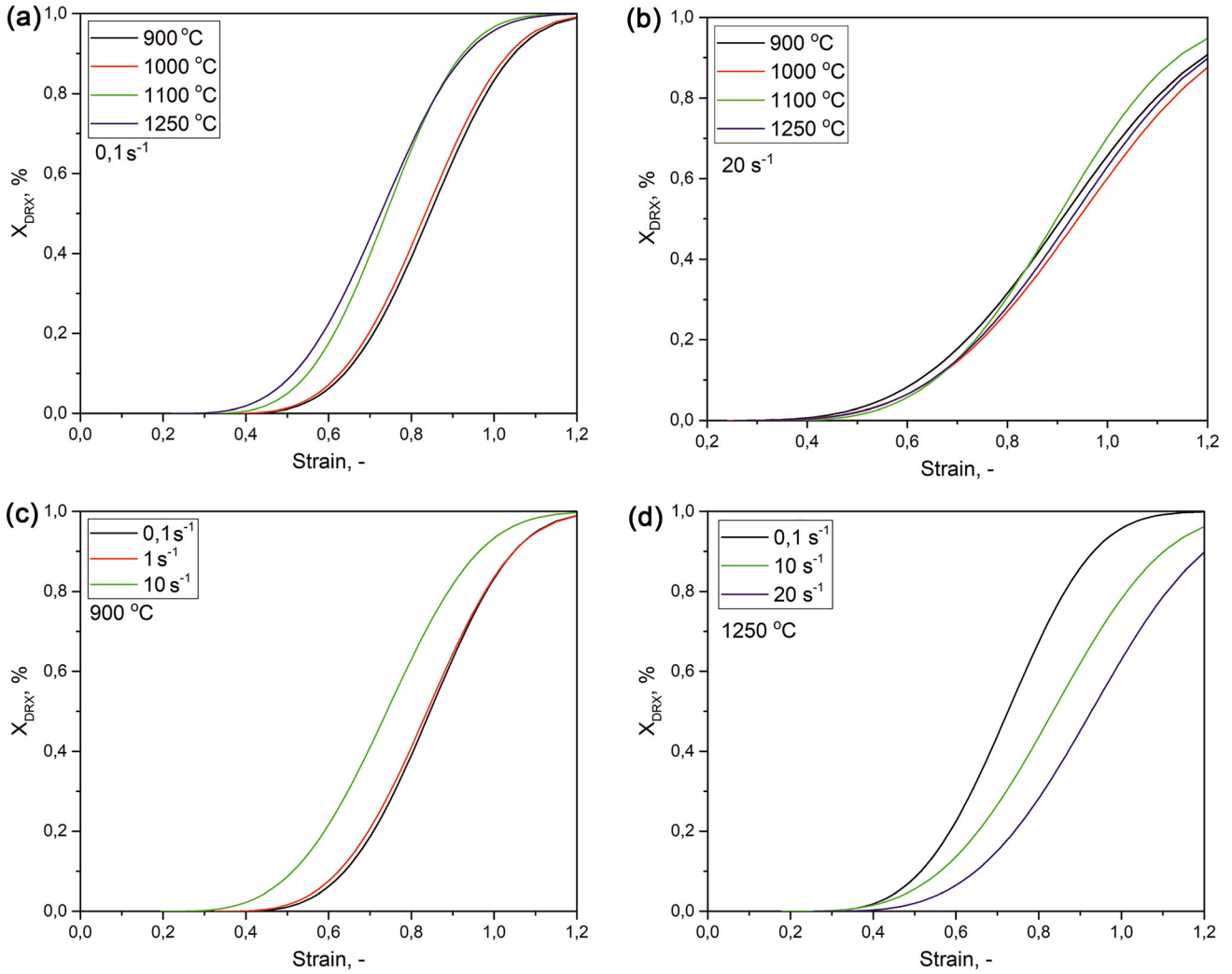
Fig. 8. Chosen volume fractions of DRX in accordance with Eq. 7 at (a) strain rate of 0.1 s^{-1} with different temperatures, (b) strain rate of 20 s^{-1} with different temperatures, (c) temperature of 900°C with different strain rates, and (d) temperature of 1250°C with different strain rates.

(Eq. 9).[49] The nature of the flow in the investigated material and the relationship between deformation conditions and high-temperature deformation activation energy can be described using:

$$Z = \dot{\varepsilon} \exp\left(\frac{Q}{RT}\right) \qquad (9)$$

$$\dot{\varepsilon} = A[\sinh(\alpha\sigma)]^n \exp\left(-\frac{Q}{RT}\right) \qquad (10)$$

where $\dot{\varepsilon}$ is strain the rate, T is the deformation temperature (K), σ is the flow stress, Q is the deformation activation energy, R is the universal gas constant (8.314 J/mol K), and A and α equal to β divided by n_1 and n, respectively, are material constants. So, the relationship between yield stress and Z can be expressed as:

$$Z = A[\sinh(\alpha\sigma)]^n \qquad (11)$$

This equation refers to the entire range of stress values and reveals an approximate hyperbolic relationship between Z and the flow stress. Applying the approach based on the hyperbolic sine function in the Arrhenius-type equation leads to a better fit between the yield stress and Z. This approach is also more universal and effective when applied across a wide range of stresses.[50] The material constants at true strain value can be calculated from:

$$n_1 = \left(\frac{\partial \ln \dot{\varepsilon}}{\partial \ln \sigma_p}\right)_T \qquad (12)$$

$$\beta = \left(\frac{\partial \ln \dot{\varepsilon}}{\partial \sigma_p}\right)_T \qquad (13)$$

$$n = \left(\frac{\partial \ln \dot{\varepsilon}}{\partial \ln\left(\sinh(\alpha\sigma_p)\right)}\right)_T \qquad (14)$$

Microstructure Prediction of 80MnSi8-6 Steel After Hot Deformation Based on Dynamic Recrystallization Kinetics and FEM Simulation

5203

Then, to estimate the material's susceptibility to initiation of DRX, the deformation activation energy Q needs to be determined for a value of ε_p, using:

$$Q = R \cdot n \cdot \left| \frac{\partial \ln(\sinh(\alpha\sigma_p))}{\partial(1/T)} \right|_\varepsilon \quad (15)$$

Applying linear regression to the relationships between $\ln\dot{\varepsilon} - \ln\sigma$ (Fig. 9a), $\ln\dot{\varepsilon} - \sigma_p$ (Fig. 9b), and $\ln\dot{\varepsilon} - \ln[\sinh(\alpha\sigma_p)]$ (Fig. 9c) as functions of deformation temperature allows the obtaining of the material constants, n, β, and n_1. Meanwhile, the linear relationship between $\ln\sinh(\sigma_p) - 1/T$ (Fig. 9d) at different deformation rates enables the calculation of the activation energy. Taking the mean value of all the slopes and multiplying by the gas constant, R, and the calculated n gives an average activation energy value of 372.1 kJ/mol. This energy must be overcome during deformation for nucleation and growth of new grains to occur. Given the values of A, α, n, and Q, Eq. 10 for the 80MnSi8-6 nanobainitic steel can be expressed as:

$$\dot{\varepsilon} = 2.05$$
$$\times 10^{14}[\sinh(0,00846\sigma_p)]^{5,24}\exp\left(-\frac{372100}{RT}\right) \quad (16)$$

The calculated average value of energy for ε_p is higher than the lattice self-diffusion activation energy of austenite, which is 270 kJ/mol.[51] The impact on the activation energy value of deformation can be influenced by deformation parameters and the strain value. Mohamadizadeh et al.[52] presented 3D activation energy maps over a wide range of temperature, strain rate, and strain value for a steel with similar carbon content. They demonstrated, among other findings, that, as deformation increases, the value of Q also increases, and the temperature has the most significant influence on the activation energy. In particular, with an increase in temperature, the value of Q decreases. Similarly, Zhao et al.[53] presented results related to activation energy values at different ranges of strain rates for low and medium carbon steels with micro-alloyed vanadium. They observed that, at higher carbon content, there is a noticeable difference in Q values between deformation in the range of $\dot{\varepsilon}$ = 0.01–1 s^{-1} and $\dot{\varepsilon}$ = 10–30 s^{-1} (292.3 kJ/mol and 475.0 kJ/mol, respectively).

Additionally, due to its relatively high carbon content, the investigated steel can be considered as high-carbon steel. Elwazri et al.[54] studied the recrystallization kinetics of high-carbon steel with micro-additions. They found that, with an increase in ε_p, the activation energy slightly increased with carbon content, but their obtained values still remained close to the lattice self-diffusion activation energy of austenite. Therefore, the high activation energy was also influenced by other alloying elements, such as vanadium, chromium, molybdenum, or manganese, as demonstrated in various studies.[5,54–56]

Average Grain Size After DRX

In order to accurately predict the grain size evolution after deformation through FEM simulations, it is necessary to establish a model for the austenite grain size after DRX. For this purpose, a modified JMAK model was considered, which is incorporated into the QForm software, and can be expressed as Eq. 17:

$$d_{DRX} = A_{gd}d_0^{M_{gd}}\dot{\varepsilon}^{L_{gd}}\exp\left(\frac{Q_{gd}}{RT}\right) \quad (17)$$

where d_{DRX} is the grain size after DRX, d_0 is the initial grain size, $\dot{\varepsilon}$ is the strain rate, Q_{gd} is the activation energy, R is the universal gas constant, T is the temperature, and A_g, L_{gd}, and M_{gd} are material constants which have been determined through linear regression, considering the grain size determined based on microstructure observations after deformation on the WUMSI simulator and rapid quenching in water. These coefficients were used during simulation of the hot compression test in the QForm software. Figure 10 presents selected microstructures with revealed PAGs. Microstructure measurements were conducted in the central section area of the sample after deformation, in a plane parallel to the deformation direction. Additionally, one sample was subjected to heat treatment according to the scheme in Fig. 1, but, instead of immediate deformation, it was quenched in water in order to determine the grain size just before deformation, which amounted to 526 μm, consistent with observations during annealing tests. Microstructure observation and the results of grain size analysis of samples after deformation showed that grain refinement occurred, regardless of the applied parameters. With increasing deformation temperature, the grain size was also larger, indicating that grain growth was also one of the mechanisms of microstructure evolution during deformation. It was also observed that, at a constant temperature, the deformation rate had no significant influence on the grain size. Therefore, the temperature was the decisive factor affecting the final grain size after deformation. Proper selection of temperature and deformation rate allows for controlling the grain size. For instance, deformation at 900°C and a rate of 20 s^{-1} gives a similar grain size as deformation at 1000°C and a rate of 10 s^{-1}.

Grain Size Prediction by FEM Simulations

The verification of developed models of grain growth, recrystallization kinetics, and grain size after DRX was conducted based on FEM simulations of hot forging, replicating the plastometric tests. To describe the behavior of the investigated
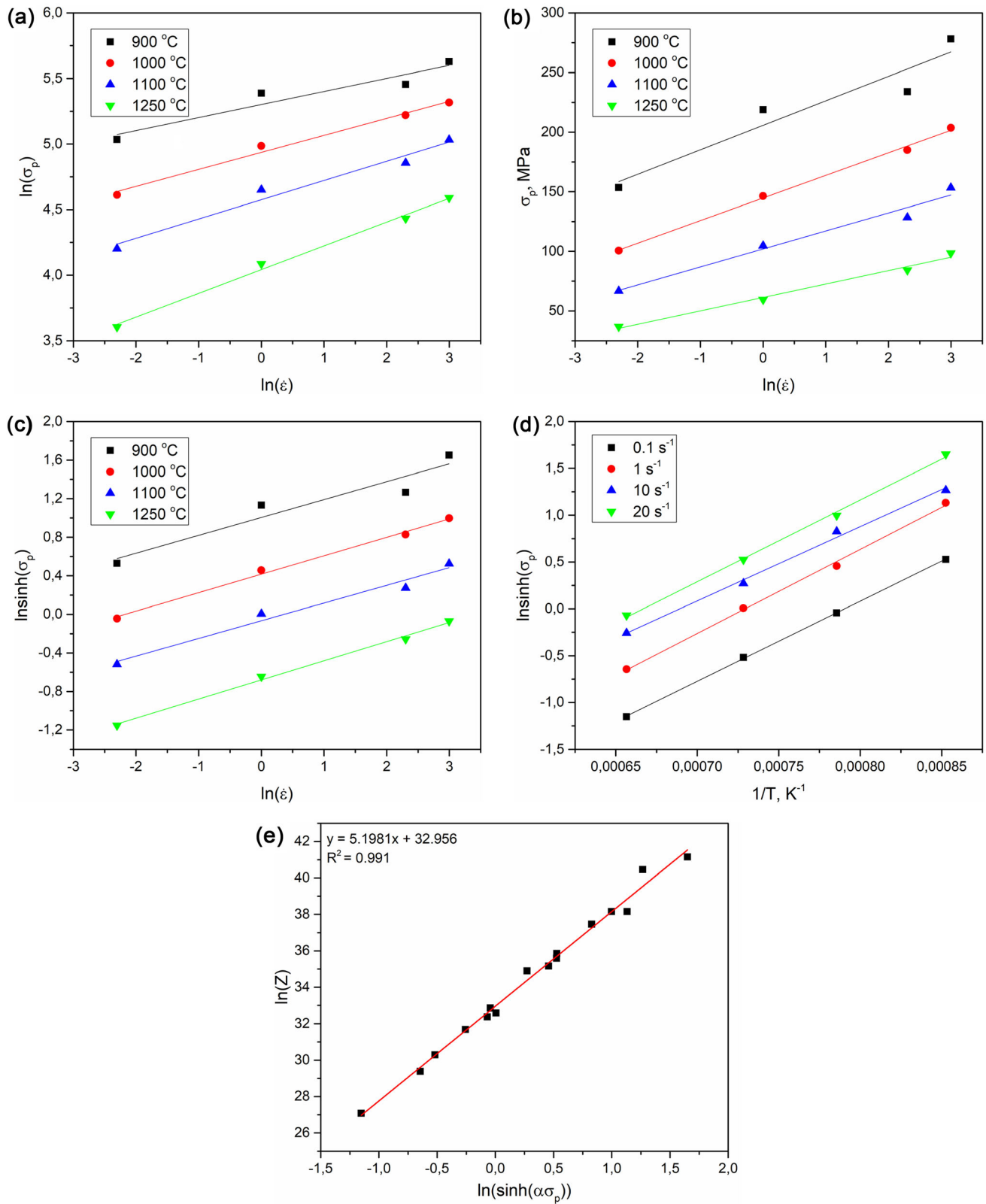
Fig. 9. The relationship between (a) $\ln\dot{\varepsilon}-\ln\sigma$, (b) $\ln\dot{\varepsilon}-\sigma_p$, (c) $\ln\dot{\varepsilon}-\ln\left[\sinh\left(\alpha\sigma_p\right)\right]$, and (d) $\ln\sinh(\sigma_p)-1/T$, and (e) $\ln(Z)-\ln\left[\sinh(\alpha\sigma_p)\right]$ for 80MnSi8-6 nanobainitic steel.

Microstructure Prediction of 80MnSi8-6 Steel After Hot Deformation Based on Dynamic
Recrystallization Kinetics and FEM Simulation

5205
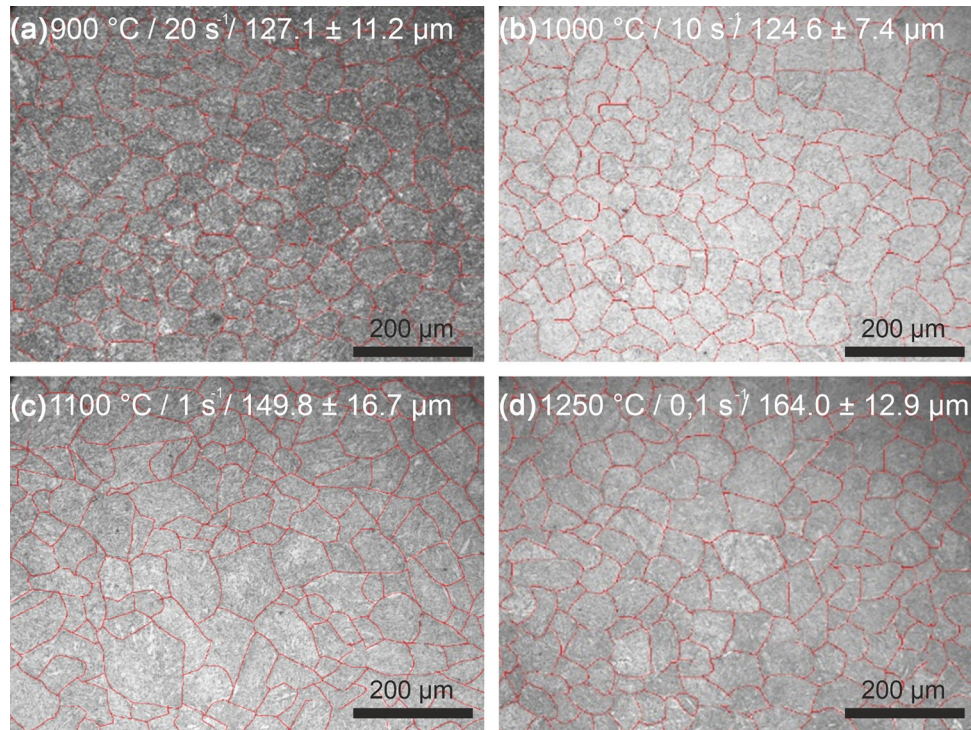
Fig. 10. Microstructures after hot deformation at (a) 900°C/20 s^{-1}, (b) 1000°C/10 s^{-1}, (c) 1100°C/1 s^{-1}, and (d) 1250°C/0.1 s^{-1} with applied PAG analysis results by Metilo$^{®}$ software.

material, flow curves were introduced into the QForm software, developed from hot compression tests, as well as the thermal characteristics of the materials determined within the range of the hot processing temperature of the studied steel. In addition to the previously described microstructure evolution models, the critical strain model, which was developed based on flow curves, was also implemented into the QForm material database. Furthermore, metadynamic recrystallization (MRX) and static recrystallization (SRX) model coefficients, along with model coefficients for average grain size after SRX or MRX, were implemented into the QForm material database, as these phenomena were identified to have a significant impact on grain size following deformation. In Tables S1–S8 in the online supplementary material, all the coefficients that have been implemented into the QFrom software database regarding the microstructure evolution of the examined steel are summarized, along with the corresponding equations. Due to the simple geometry of the sample, a 2D axisymmetric process was simulated. The sample had a diameter of 10 mm and a height of 18 mm and was deformed to a strain value of 1.2. The simulation was conducted at a constant ambient and tool temperature, which was equal to the deformation temperature of the material in the given simulation variant. The implemented tool speed replicated the displacement characteristics at a constant strain rate. Since, in the actual process, the samples were heated in steel containers in an external furnace, and then

removed from the containers and cooled in water, which takes a certain amount of time, 5 s of holding before and 10 s after the compression during the simulation were added to each. A friction factor of 0.4 was assumed between the material and the tools, corresponding to the use of a graphite lubricant.

Figures 11 and 12 show exemplary simulation results for two combinations of hot forging parameters: 1000°C temperature and 10 s^{-1} strain rate, and 1250°C temperature and 0.1 s^{-1} strain rate. The distribution of strain intensity (Figs. 11a and 12a) is typical for hot compression tests, regardless of the applied parameter combination. In both cases, the occurrence of strain inhomogeneity is observed. The highest intensity is noted at the center of the sample cross-section, and lower intensities are observed at the surfaces in contact with the tools, which is naturally a consequence of friction between the material and the tools. The distributions of strain intensity between the two considered variants differ only slightly, mainly due to the different strain rates and deformation temperatures.

In cross-sectional areas where the strain intensity was low, recrystallization occurred to a small extent or not at all, if the required critical strain was not exceeded (Figs. 11b and 12b). In the center of the sample cross-sections, the high strain value resulted in near 100% DRX fraction. Additionally, the distribution of grain size is closely linked to the distribution of DRX fraction. As expected, where a higher percentage of DRX occurred, the grain size
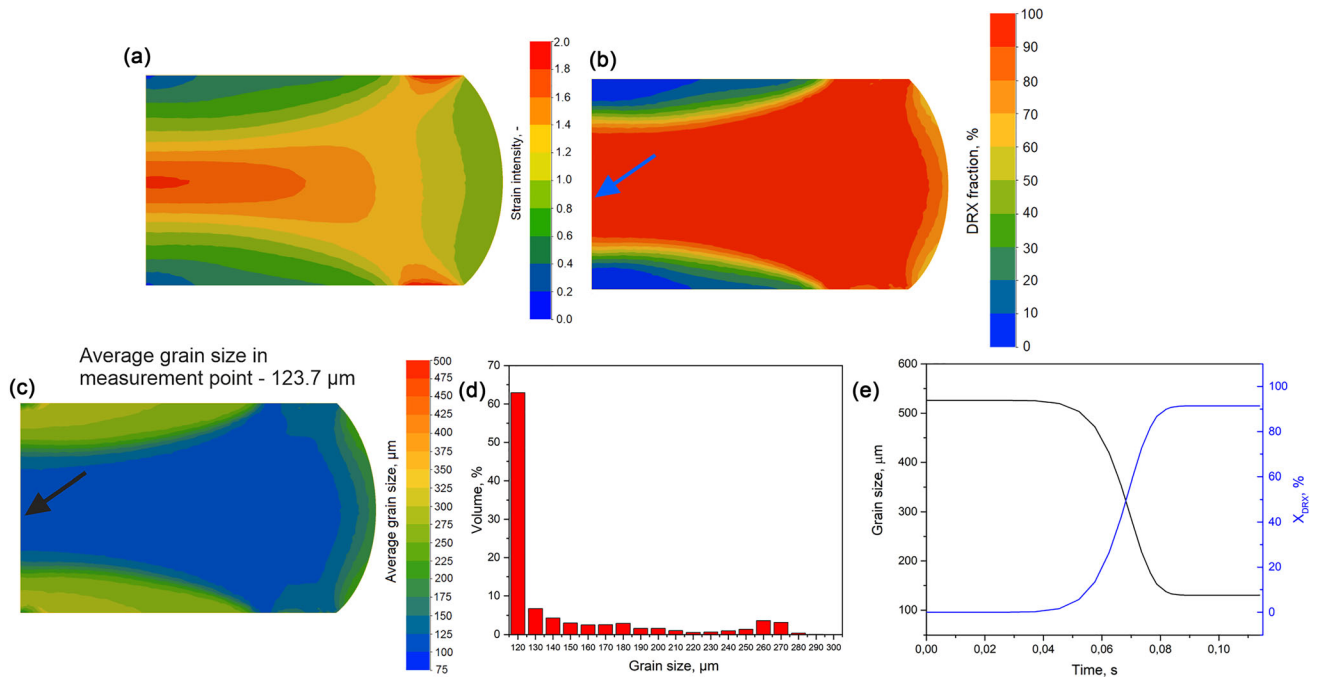
Fig. 11. Hot compression simulation results for temperature of 1000°C and strain rate of 10 s^{-1}: (a) strain intensity distribution, (b) DRX fraction distribution, (c) average grain size distribution, (d) distributions of grain size, (e) change of grain size and DRX fraction over the time of simulation; blue and black arrows the measurement points of the DRX fraction and grain size (Color figure online).
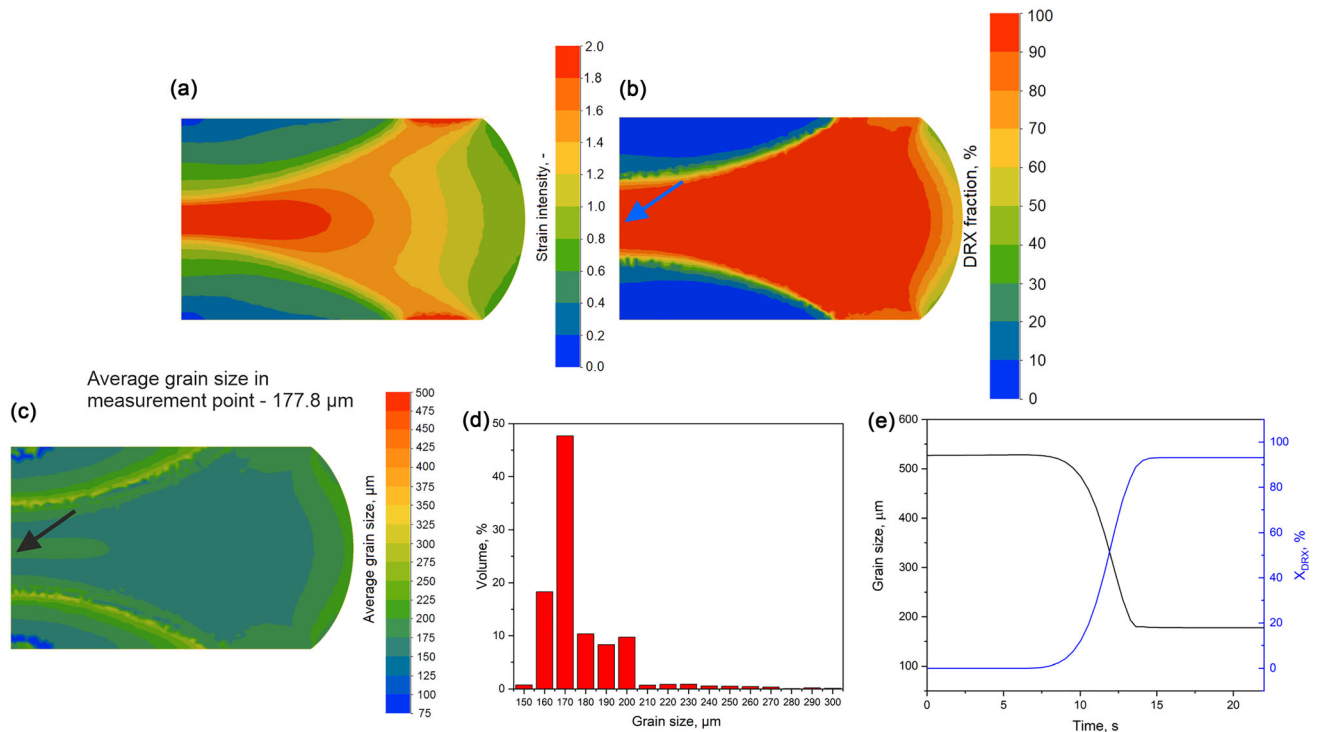

Fig. 12. Hot compression simulation results for temperature of 1250°C and strain rate of 0.1 s^{-1}: (a) strain intensity distribution, (b) DRX fraction distribution, (c) average grain size distribution, (d) distributions of grain size, (e) change of grain size and DRX fraction over the time of simulation; blue and black arrows the measurement points of the DRX fraction and grain size (Color figure online).

was finer. It can be observed that, for the temperature of 1000°C, the DRX fraction reached a higher value compared to the 1250°C temperature of

forging (Figs. 11e and 12e) and covered a broader range (Figs. 11b and 12b), which resulted in a more uniform distribution of the dynamically

recrystallized fraction and grain size over the cross-section of the sample. For a temperature of 1250°C, a higher intensity of material flow is seen in the middle part of the sample, and a lower intensity is seen at the point of contact between the material and the tool.

The cross-sectional views of the numerically calculated austenitic microstructure after complete recrystallization following hot compression at 1000°C and a strain rate of 10 s^{-1}, as well as at 1250°C and a strain rate of 0.1 s^{-1}, are shown in Figs. 11c and 12c, respectively. By comparing the obtained grain size from the measurement point located at the center of the cross-section of the forged sample, in a plane parallel to the direction of forging, with the results of the experimental measurements, it can be concluded that the simulation is in good agreement with the experiment. For variant 1250°C/0.1 s^{-1}, during the simulation, a grain size value of 177.8 μm was recorded at the measurement point, whereas the experimental measurement showed a value of 164.0 μm. On the other hand, for variant 1000°C/10 s^{-1}, an even better agreement was achieved. Simulation results at the measurement point revealed a grain size of 123.7 μm compared to 124.6 μm, determined from microstructure observations. In addition, Figs. 11d and 12d show the distributions of grain size on the section after hot compression simulation. It can be seen that in both the considered cases the grain distribution is relatively uniform and in agreement with the determined grain size at the measuring point. This is because the DRX covered most of the volume of the sample, excluding the areas near the contact surface with the tool. Figure 13 shows a comparison of the simulation and experimental test results for all combinations of hot compression parameters. Considering all 16 investigated simulation variants, the average percentage error in grain size was 8.3 ± 5.4%.

The developed models for the microstructure evolution of 80MnSi8-6 steel, implemented into FEM software, were successfully verified through a comparison of simulation results with the analysis of the grain size of the samples after hot compression tests. Industrial hot deformation processes of steel are commonly carried out at the temperature of stable austenite. Therefore, the austenite grain size plays a crucial role in tailoring the strength properties of the final product. Understanding the kinetics of evolution in the microstructure during hot deformation and the ability to control the austenite grain size are invaluable assets for industrial partners producing steel products. Modeling hot deformation processes with simultaneous simulation of grain size changes allows for time and cost savings for industrial companies when implementing the processing of new materials or optimizing previously designed technologies. With knowledge of microstructure evolution models, it is possible to replace time-consuming and costly laboratory and technological trials using FEM simulations.

The presented results can be valuable for industries producing products not only from nanobainitic steels but also from high-carbon alloy steels. The developed models can be successfully applied to simulate more complex hot deformation processes of the investigated steel and grades of similar chemical composition under various temperature conditions and applied strain rates.
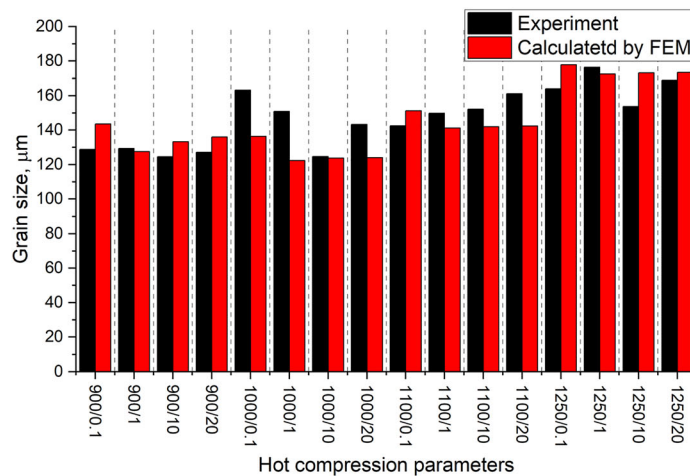
	900/0.1	900/1	900/10	900/20	1000/0.1	1000/1	1000/10	1000/20	1100/0.1	1100/1	1100/10	1100/20	1250/0.1	1250/1	1250/10	1250/20	Average
Difference, μm	14.8	1.8	8.8	8.9	26.8	28.5	0.9	9.3	8.7	8.6	10.2	18.8	13.8	4	19.4	4.4	12.4 ± 8.4
Average percentage error, %	11.5	1.4	7.1	7	16.4	18.9	0.7	13.5	6.1	5.7	6.7	11.7	8.4	2.3	12.6	2.6	8.3 ± 5.4

Fig. 13. Comparison of the PAG average grain size in the center of the sample cross-section after hot compression tests and simulation, and the difference between the grain size results and the average percentage error.

CONCLUSION

The effects of deformation parameters on the microstructure evolution behavior in 80MnSi8-6 steel were investigated at temperatures of 900–1250°C and strain rates of 0.1–20 s^{-1}. The Arrhenius equation was developed based on the true stress–strain curves. Grain growth and DRX kinetic models were developed, as well as grain size after the DRX model and verified by FEM simulations of the compression tests. The following conclusions were drawn:

(1) The microstructures of 80MnSi8-6 steel annealed at different temperatures show an increase in grain size with temperature and annealing time. The modeled grain growth kinetics for different austenitizing temperatures and times were in agreement with experimental data, except for holding at 1250°C where an intense grain growth was observed.

(2) The flow curves demonstrate that the investigated material exhibits typical strain rate and temperature sensitivity. Based on them, it was possible to develop a constitutive equation for the examined steel, expressed as: $\dot{\varepsilon} = 2.05 \times 10^{14} \left[\sinh \left(0,00846 \sigma_p \right) \right]^{5,24}$-, as well as a DRX model known as the S-type relationship, which was later used in the FEM simulations.

(3) Analysis of the S-curves showed that lowering the temperature delays the onset of recrystallization, increasing the required critical strain. On the other hand, higher temperatures result in faster recrystallization due to a lower critical strain. At lower temperatures, the strain rate significantly influences the DRX rate, where energy delivered by high strain rates outweighs the influence of temperature. At higher temperatures, DRX occurs earlier even at low strain rates due to increased energy and dislocation density.

(4) Microstructure observations after deformation confirm that grain refinement occurred regardless of the applied parameters. Higher deformation temperatures resulted in larger grain sizes, indicating simultaneous grain growth. Modification of deformation temperature has a greater effect on the final grain size than change in the strain rate.

(5) Developed models for grain growth, recrystallization kinetics, and grain size after DRX were validated using FEM simulations of hot compression, replicating laboratory plastometric tests. Grain size distribution for all combinations of deformation parameters were calculated using FEM. Comparison of computed grain size with experimental measurements showed good agreement, and the average percentage error was 8.3 ± 5.4%.

SUPPLEMENTARY INFORMATION

ACKNOWLEDGEMENTS

DATA AVAILABILITY

Data will be made available on request.

CONFLICT OF INTEREST

The authors declare that they have no conflict of interest.

OPEN ACCESS

REFERENCES

1. M. Graf, M. Ullmann, G. Korpala, H. Wester, B. Awiszus, R. Kawalla, and B.A. Behrens, *Metals (Basel)* 8, 1 (2018).
2. X. Wang, K. Chandrashekhara, S.N. Lekakh, D.C. Van Aken, and R.J. O'Malley, *Steel Res. Int.* 90, 1 (2019).
3. O. Lypchanskyi, T. Śleboda, K. Zyguła, M. Wojtaszek, and M. Rumiński, *Procedia Manuf.* 50, 63 (2020).
4. J. Gai, J. Cheng, J. Li, Z. Du, W. Zhang, S. Yu, and Z. Yu, *Front. Mater.* 6, 1 (2020).
5. G. Liu, C. Mao, R. Ding, L. Yu, C. Liu, and Y. Liu, *J. Nuclear Mater.* 557, 153285 (2021).
6. P. Guo, L. Deng, X.Y. Wang, and J.J. Li, *Sci. China Technol. Sci.* 62, 1534 (2019).
7. S. Kumar, B. Aashranth, D. Samantaray, M.A. Davinci, U. Borah, and A.K. Bhaduri, *Vacuum* 156, 20 (2018).
8. X. Yang, J. Zhao, X. Yan, X. Shi, and H. Guo, *High Temp. Mater. Process.* 41, 669 (2022).
9. H. Mirzadeh, *J. Mater. Res. Technol.* 25, 7050 (2023).
10. M. Moghaddam, A. Zarei-Hanzaki, E. Farabi, and M. Taheri-Mandarjani, *Adv. Eng. Mater.* 18, 989 (2016).
11. K. Zyguła, M. Wojtaszek, T. Śleboda, O. Lypchanskyi, M. Rumiński, G. Korpała, and U. Prahl, *Procedia Manuf.* 50, 546 (2020).

12. Z. Nasiri, S. Ghaemifar, M. Naghizadeh, and H. Mirzadeh, *Met. Mater. Int.* 27, 2078 (2021).
13. M. Wojtaszek, Ł Lisiecki, A. Łukaszek-Sołek, G. Korpała, K. Zyguła, T. Śleboda, M.B. Jabłońska, and U. Prahl, *Arch. Civ. Mech. Eng.* 23, 240 (2023).
14. X.Y.H. Wu, Y. Gu, R. Yuan, and Y.Z.Y. Feng, *J. Iron. Steel Res. Int.* 29, 647 (2022).
15. A. Kumar and A. Singh, *Materialia* 15, 101034 (2021).
16. C. Garcia-Mateo, F.G. Caballero, and H.K.D.H. Bhadeshia, *ISIJ Int.* 43, 1238 (2003).
17. H. Yang and H.K.D.H. Bhadeshia, *Mater. Sci. Technol.* 24, 335 (2008).
18. C. Garcia-Mateo, F.G. Caballero, and H.K.D.H. Bhadeshia, *ISIJ Int.* 43, 1821 (2003).
19. M. Soliman and H. Palkowski, *Arch. Civ. Mech. Eng.* 16, 403 (2016).
20. H.K.D.H. Bhadeshia, *Proc. R. Soc. A Math. Phys. Eng. Sci.* 466, 3 (2010).
21. C. Garcia-Mateo, G. Paul, M.C. Somani, D.A. Porter, L. Bracke, A. Latz, C.G. de Andres, and F.G. Caballero, *Metals (Basel)* 7, 159 (2017).
22. S. Chatterjee, H.S. Wang, J.R. Yang, and H.K.D.H. Bhadeshia, *Mater. Sci. Technol.* 22, 641 (2006).
23. M. Liu, G. Xu, J. Tian, Q. Yuan, M. Zhou, and H. Hu, *Steel Res. Int.* 90, 1 (2019).
24. H.K.D.H. Bhadeshia, *Bainite in Steels* (CRC Press, Boca Raton, 2019).
25. M. Szala, *ITM Web Conf.* 15, 06003 (2017).
26. A.N. Levanov, *J. Mater. Process. Technol.* 72, 314 (1997).
27. F. Najafkhani, S. Kheiri, B. Pourbahari, and H. Mirzadeh, *Arch. Civ. Mech. Eng.* 21, 1 (2021).
28. A. Reshetov, O. Bylya, N. Stefani, M. Rosochowska, and P. Blackwell, *Proceedings of the 13th Intenational Symposium of Superalloys*, p. 531 (2016).
29. A.I. Fernández, P. Uranga, B. López, and J.M. Rodriguez-Ibabe, *Mater. Sci. Eng. A* 361, 367 (2003).
30. L. Wang, D. Qian, J. Guo, and Y. Pan, *Adv. Mech. Eng.* 5, 762890 (2013).
31. L. Duan, J. Wang, Q. Liu, X. Sun, and J. Cao, *J. Iron. Steel Res. Int.* 17, 62 (2010).
32. W. Li and K. Xia, *Mater. Sci. Eng. A* 329–331, 430 (2002).
33. A.B. Cota, C.A.M. Lacerda, F.L.G. Oliveira, F.A. Machado, and F.G. Da Silva Araújo, *Scr. Mater.* 51, 721 (2004).
34. L. Zhang and T. Kannengiesser, *Mater. Sci. Eng. A* 613, 326 (2014).
35. T.M. Ivaniski, P.J. de Castro, D. Rodrigues, J. Épp, R.M. Nunes, and Ad.S. Rocha, *Mater. Res.* 25, e20210598 (2022).
36. A. Królicka, K. Radwański, A. Ambroziak, and A. Żak, *Mater. Sci. Eng. A* 768, 138446 (2019).
37. S.J. Lee and Y.K. Lee, *Mater. Des.* 29, 1840 (2008).
38. R. Staśko, H. Adrian, and A. Adrian, *Mater Charact* 56, 340 (2006).
39. C. Menapace, N. Sartori, M. Pellizzari, and G. Straffelini, *J. Eng. Mater. Technol.* 140, 1 (2018).
40. A.M. Ravi, A. Kumar, M. Herbig, J. Sietsma, and M.J. Santofimia, *Acta Mater.* 188, 424 (2020).
41. D. Gomez-Marquez, E. Ledesma-Orozco, R. Hino, E. Aguilera-Gomez, G. Korpała, and U. Prahl, *SN Appl. Sci.* 4, 220 (2022).
42. P. Christiansen, P.A.F. Martins, and N. Bay, *Exp. Mech.* 56, 1271 (2016).
43. E.I. Poliak and J.J. Jonas, *Acta Mater.* 44, 127 (1996).
44. L. Wang, F. Liu, Q. Zuo, and C.F. Chen, *Mater. Des.* 47, 737 (2013).
45. L. Wang, L. Ji, K. Yang, X. Gao, H. Chen, and Q. Chi, *Materials (Basel)* 15, 7356 (2022).
46. G.Z. Quan, G.S. Li, T. Chen, Y.X. Wang, Y.W. Zhang, and J. Zhou, *Mater. Sci. Eng. A* 528, 4643 (2011).
47. S. Mandal, M. Jayalakshmi, A.K. Bhaduri, and V. Subramanya Sarma, *Metall. Mater. Trans. A Phys. Metall. Mater. Sci.* 45, 5645 (2014).
48. H. Jiang, J. Dong, M. Zhang, and Z. Yao, *Metall. Mater. Trans. A Phys. Metall. Mater. Sci.* 47, 5071 (2016).
49. G. Ji, F. Li, Q. Li, H. Li, and Z. Li, *Mater. Sci. Eng. A* 527, 2350 (2010).
50. Z. Cai, H. Ji, W. Pei, X. Tang, X. Huang, and J. Liu, *Vacuum* 165, 324 (2019).
51. S. Saadatkia, H. Mirzadeh, and J.M. Cabrera, *Mater. Sci. Eng. A* 636, 196 (2015).
52. A. Mohamadizadeh, A. Zarei-Hanzaki, and H.R. Abedi, *Mech. Mater.* 95, 60 (2016).
53. H. Zhao, J. Qi, G. Liu, R. Su, and Z. Sun, *J. Mater. Res. Technol.* 9, 11319 (2020).
54. A.M. Elwazri, P. Wanjara, and S. Yue, *Mater. Sci. Eng. A* 339, 209 (2003).
55. Z. Guo and L. Li, *Mater. Des.* 89, 665 (2016).
56. S.F. Medina and J.E. Mancilla, *ISIJ Int.* 36, 1063 (1996).